Gaining insights into API dispersion in hot melt extrusion using Raman spectroscopy and scanning electron microscopy

Introduction

Hot-melt extrusion (HME) is used to prepare solid dispersions of poorly soluble active pharmaceutical ingredients (APIs) and for creating controlled-release medications.[1] In this process, APIs are compounded with thermoplastic polymers and extruded to form a solid dispersion. The polymer matrix acts as a solid solvent for the drug molecules. Amorphous API dispersions in a polymer matrix at the molecular level are highly desirable from a solubility enhancement perspective because the drug is in a dissolved molecular state with no lattice energy to overcome prior to dissolution. Furthermore, amorphous API dispersions can provide a physical barrier to aggregation of drug particles and reduce the risk of physical change post-manufacture.

Characterisation of hot-melt extrudates is an integral part of the overall HME process design and optimisation. Various analytical techniques have been used to investigate the physicochemical factors relevant to HME.[2–5] Terahertz (THz) Raman imaging can characterise the solid physical states of acetaminophen (APAP) in a hydroxypropyl methylcellulose (HPMC) matrix prepared by HME.[6] It has been demonstrated that Raman imaging analysis can distinguish crystalline and amorphous APAP based on the Raman features in the THz region and offers a direct visualisation of the APAP distribution in HPMC through correlation profiling; though the spatial resolution of Raman imaging is limited to approximately 1µm. Using electrons as the radiation source, scanning electron microscopy (SEM) offers a higher spatial resolution (in nm scale) than other optical techniques. The large depth-of-field of SEM also yields images with a characteristic three-dimensional (3D) appearance that aids understanding of the surface structure of a sample. SEM has been used to investigate the formation of solid dispersions in HME by probing the surface morphology of extrudates, especially the crystalline structure. By correlating molecular-level interactions and solid physical state changes with morphological variations, the combination of Raman imaging and SEM provides a holistic insight into the multifaceted HME process.

We report herein the use of THz Raman imaging and SEM to investigate the solid physical states of APAP in an HPMC matrix prepared by HME. Extrudates from two different HME processes of different screw speeds are analysed and compared. The impact of screw speed on the formation of solid dispersions is also rationalised.

Figure 1

Thermo Scientific DXR3xi Raman Imaging Microscope

Experimental

Materials

Acetaminophen (APAP; Spectrum Chemicals, Gardena, CA), a crystalline BCS I drug with a melting point of 169–170°C was chosen as the model API. Hydroxypropyl methylcellulose (HPMC; Ashland, Wilmington, DE) E5 was used as the polymer matrix.

Hot-melt extrusion

An 11mm twin-screw extruder, Thermo Scientific Process 11 (Thermo Fisher Scientific, Karlsruhe, Germany), was used for the HME processes. Samples were withdrawn from two different 'stages' of the mixing, conveying and discharge zone: an early stage, where minimal processing has occurred and a late stage where significant processing has occurred.

The blending ratio of APAP and HPMC was 30:70 (w/w). Two different HME processes were performed with two different screw speeds. For each HME process, small amounts of sample were withdrawn when the extrusion reached the steady state and after the extruder was stopped. The samples were then pressed into thin films using a hydraulic press with heating panels at 40°C to be analysed by Raman imaging and SEM.

Raman imaging

Raman imaging was performed using a Thermo Scientific DXR3xi Raman Imaging Microscope (**Figure 1**), using a 532nm laser operated at 8mW power at the sample. Data acquisition and processing were carried out using the Thermo Scientific OMNICxi software. Raman images were obtained by the Correlation Profiling option of the OMNICxi software, using the THz region (≤200cm^{-1}) of the crystalline APAP Raman spectrum as a reference.

The correlation profile shows the correlation between the spectrum at each pixel (sampling point) in the Raman image and the specified reference spectrum. The higher the intensity value, the greater similarity to the reference spectrum. A value of 1.0 indicates that the sample spectrum and reference spectrum are identical and is displayed in red. For the purpose of direct comparison, a correlation range of 0.75-1 was applied to each Raman image.

SEM imaging

All SEM images were acquired using a Thermo Scientific Phenom XL Desktop SEM equipped with a CeB6 source and a Thermo Scientific Phenom Pharos Desktop SEM equipped with an FEG source. The SEM images were acquired with a solid-state back-scattered electron

Figure 2

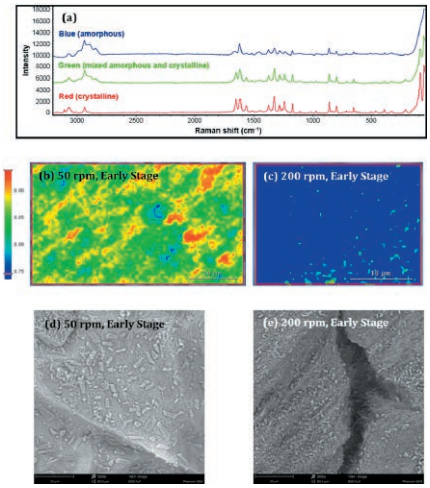

a: Representative Raman spectra from the blue, green and red regions from subsequent Raman images. **b-c:** Raman images of the samples from the early stage using two different screw speeds, 50 and 200 rpm. The images were obtained using a 100× microscope objective and a 0.5 µm pixel size. **d-e:** SEM images of the same samples obtained using a 3000× magnification.

detector (BSD) sensitive to atomic number variations. Due to the non-conductive nature of the extrudates, the low vacuum setting of 60Pa was used for all experiments to avoid charging artefacts. The acceleration voltage was set to 10kV and the spot size was kept to a medium value, allowing high-resolution imaging with sufficient signal-to-noise ratio.

Results and discussion

Figure 2a shows the representative Raman spectra of amorphous (blue trace), partially amorphous (green trace) and crystalline APAP (red trace). In the THz Raman region, there is a strong sharp peak at 89cm^{-1} unique to the crystalline APAP, which can be ascribed to the crystalline lattice vibrations (phonon mode).

It is also noted that the spectra of the amorphous region and the partially-amorphous region both contain significant contributions from the polymeric matrix, whereas the spectrum of the crystalline region does not.

Figures 2b-c show the Raman images of the samples withdrawn from the early stage. When a lower screw speed of 50rpm is used (**Figure 2b**), the sample contains primarily partially-amorphous dispersion (green regions) and crystalline APAP (red regions), with minute amorphous dispersion (blue regions). In contrast, the sample formed using higher screw speeds (**Figure 2c**) consists of predominantly amorphous dispersion (blue regions), noticeable partially-amorphous dispersion (green regions) and negligible crystalline APAP (red regions). These observations are corroborated by the corresponding SEM images (**Figure 2d-e**). The low screw speed sample (**Figure 2d**) exhibits appreciable amounts of well-defined, rectangular crystal structures (crystalline APAP) as well as some smaller, irregular particles (partially-amorphous solid dispersion). The sizes of these morphological features range from sub-µm to 15µm. The high screw speed sample (**Figure 2e**), however, exhibits more irregular shaped particles ranging from sub-µm to approximately 2µm in size. The compounding step of an HME process involves distributive mixing, where the API is distributed throughout the whole polymer matrix, and dispersive mixing, where more shear stress is applied to break down agglomerates. The energy imparted by the friction between screws and extruded material at 50rpm was not enough to completely overcome the crystal lattice energy; hence, the prevalence of partially-amorphous solid dispersion and crystalline APAP. Conversely, a high screw speed of 200rpm is conducive to both distributive and dispersive mixing and facilitates the formation of desirable amorphous and partially-amorphous solid dispersion.

Figures 3a-b show the Raman images of the samples from two different stages using a high screw speed (200rpm). At the early stage (**Figure 3a**), the APAP was present in both partially-amorphous solid dispersion (green regions) and amorphous solid dispersion (blue regions); whereas the late-stage sample (**Figure 3b**) exhibits near-uniform, amorphous solid dispersions (blue regions). These observations are consistent with the SEM results (**Figure 3c-d**). The early-stage sample (**Figure 3c**) shows partially-amorphous solid dispersions, whereas the late-stage sample (**Figure 3d**) exhibits a uniform and homogeneously mixed mass with wrinkled surface, indicating a near-complete amorphous dispersion.

Figure 3

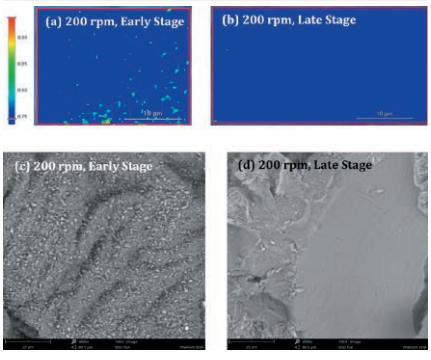

a-b: Raman images of the samples from the early and late stages using a screw speed of 200 rpm. The images were obtained using a 100× microscope objective and a 0.5 µm pixel size. **c-d:** SEM images of the same samples obtained using a 3000× magnification.

Conclusions

Extrudates from two different HME processes of different screw speeds were compared using Raman imaging and SEM. At the early stage of the extrusion, a low screw speed results in partially-amorphous dispersion and crystalline APAP whereas a high screw speed process leads to predominantly amorphous and partially-amorphous dispersion. At the late stage, high screw speed samples exhibit a uniform and homogeneously mixed surface indicative of a near-complete amorphous dispersion; whereas low screw speed extrudates display a dense surface with pockets of both crystalline APAP and partially-amorphous APAP dispersions.

Both Raman imaging and SEM analyses confirm that high screw speed favours the formation of amorphous APAP solid dispersion. While Raman imaging provides molecular-level insight to the underlying chemistry of an HME process by adding chemical annotation to the optical image, SEM excels in spatial resolution to monitor the particle size reduction in HME, especially in the sub-µm scale, which is critical in order to understand the solid physical state transformation of the API in HME.

References

1. M.A. Repka, S. Bandari, V.R. Kallakunta, A.Q. Vo, H. McFalla, M.B. Pimparade, and A.M. Bhagurkar, Int. J. Pharm. 535, 68–85 (2018).
2. R. Censi, M.R. Gigliobianco, Cr. Casadidio, and P. Di Martino, Pharmaceutics 10, 89 (2018).
3. S. Baghel, H. Cathcart, and N.J. O'Reilly, J. Pharm. Sci. 105, 2527-2544 (2016).
4. P. Hitzer, T. Bäuerle, T. Drieschner, E. Ostertag, K. Paulsen, H. van Lishaut, G. Lorenz, and K. Rebner, Anal. Bioanal. Chem. 409, 4321–4333 (2017).
5. N. Furuyama, S. Hasegawa, T. Hamaura, S. Yada, H. Nakagami, E. Yonemochi, and K. Terada, Int. J. Pharm. 361, 12–18 (2008).
6. Mohammed Ibrahim, Jiaxiang Zhang, Michael Repka, and Rui Chen, AAPS PharmSciTech 20, 62 (2019).